First Observations of Large Scale Traveling Ionospheric Disturbances Using Automated Amateur Radio Receiving Networks

Nathaniel Anthony Frissell[1,1], Stephen Roland Kaeppler[2,2], Diego F Sanchez[3,3], Gareth William Perry[3,3], William Dozier Engelke[4,4], Philip J Erickson[5,5], Anthea J Coster[6,6], John Michael Ruohoniemi[7,7], J. B. H. Baker[7,7], and Mary Lou West[8,8]

[1]The University of Scranton
[2]Clemson University
[3]New Jersey Institute of Technology
[4]The University of Alabama
[5]Massachusetts Institute of Technology
[6]MIT Haystack Observatory
[7]Virginia Tech
[8]Montclair State University

November 30, 2022

Abstract

We demonstrate a novel method for observing Large Scale Traveling Ionospheric Disturbances (LSTIDs) using high frequency (HF) amateur radio reporting networks, including the Reverse Beacon Network (RBN), Weak Signal Propagation Reporter Network (WSPRNet), and PSKReporter. LSTIDs are quasi-periodic variations in ionospheric densities with horizontal wavelengths > 1000 km and periods between 30 to 180 min. On 3 Nov 2017, LSTID signatures were observed simultaneously over the continental United States in amateur radio, SuperDARN HF radar, and GNSS Total Electron Content with a period of ~2.5 hr, propagation azimuth of ~163°, horizontal wavelength of ~1680 km, and phase speed of ~1200 km/hr. SuperMAG SME index enhancements and Poker Flat Incoherent Scatter Radar measurements suggest the LSTIDs were driven by auroral electrojet intensifications and Joule heating. This novel measurement technique has applications in future scientific studies and for assessing the impact of LSTIDs on HF communications.

First Observations of Large Scale Traveling Ionospheric Disturbances Using Automated Amateur Radio Receiving Networks

Nathaniel A. Frissell[1], Stephen R. Kaeppler[2], Diego F. Sanchez[3], Gareth W. Perry[3], William D. Engelke[4], Philip J. Erickson[5], Anthea J. Coster[5], J. Michael Ruohoniemi[6], Joseph B. H. Baker[6], and Mary Lou West[7]

[1]Department of Physics and Engineering, The University of Scranton, Scranton, PA, USA
[2]Department of Physics and Astronomy, Clemson University, Clemson, SC, USA
[3]Center for Solar-Terrestrial Research, New Jersey Institute of Technology, Newark, NJ, USA
[4]Center for Advanced Public Safety, University of Alabama, Tuscaloosa, AL, USA
[5]Haystack Observatory, Massachusetts Institute of Technology, Westford, MA, USA
[6]Bradley Department of Electrical and Computer Engineering, Virginia Tech, Blacksburg, VA, USA
[7]Department of Physics and Astronomy, Montclair State University, Montclair, NJ, USA

Key Points:

- Amateur radio data provides a new method for studying Large Scale Traveling Ionospheric Disturbances and HF communications impacts
- Large Scale Traveling Ionospheric Disturbances are seen for the first time simultaneously in amateur radio, SuperDARN, and GNSS TEC data
- Observed midlatitude Large Scale Traveling Ionospheric Disturbances are likely driven by auroral zone electrojet surges and Joule heating

Corresponding author: Nathaniel A. Frissell, `nathaniel.frissell@scranton.edu`

Abstract

We demonstrate a novel method for observing Large Scale Traveling Ionospheric Disturbances (LSTIDs) using high frequency (HF) amateur radio reporting networks, including the Reverse Beacon Network (RBN), Weak Signal Propagation Reporter Network (WSPRNet), and PSKReporter. LSTIDs are quasi-periodic variations in ionospheric densities with horizontal wavelengths $>$ 1000 km and periods between 30 to 180 min. On 3 Nov 2017, LSTID signatures were observed simultaneously over the continental United States in amateur radio, SuperDARN HF radar, and GNSS Total Electron Content with a period of $\sim$2.5 hr, propagation azimuth of $\sim$163°, horizontal wavelength of $\sim$1680 km, and phase speed of $\sim$1200 km hr^{-1}. SuperMAG SME index enhancements and Poker Flat Incoherent Scatter Radar measurements suggest the LSTIDs were driven by auroral electrojet intensifications and Joule heating. This novel measurement technique has applications in future scientific studies and for assessing the impact of LSTIDs on HF communications.

Plain Language Summary

Large Scale Traveling Ionospheric Disturbances (LSTIDs) are variations in the ionosphere with wavelengths greater than 1000 kilometers, periodicities between 30 minutes to 3 hours, and speeds greater than about 1400 kilometers per hour. Auroral zone disturbances are generally cited as the energy source for LSTIDs. In this paper, we show for the first time that LSTIDs can cause variations in the distances amateur (ham) radio operators can communicate using data from the Reverse Beacon Network (RBN), Weak Signal Propagation Reporter Network (WSPRNet), and PSKReporter amateur radio networks. The LSTID signatures in the amateur radio data are in excellent agreement with LSTID observations from two well-established instruments: the Blackstone, Virginia SuperDARN radar and a large scale network of GNSS based ionospheric Total Electron Content receivers. The observed LSTIDs appear 2 to 3 hours after auroral zone disturbances are detected by ground magnetometers in the SuperMAG network and the Poker Flat Incoherent Scatter Radar (PFISR) in Alaska. Results suggest that auroral zone disturbances were the ultimate cause of the observed LSTIDs. This paper provides a foundation for using large-scale, crowd-sourced amateur radio observations of LSTIDs as a new method for the study of LSTIDs.

1 Introduction

Traveling ionospheric disturbances (TIDs) are quasi-periodic variations of ionospheric densities in Earth's upper atmosphere, believed to be the ionospheric signatures of atmospheric gravity waves (AGWs) (Hines, 1960). TIDs are generally categorized as either Large Scale TIDs (LSTIDs, horizontal speeds between 400 to 1000 m s^{-1}, periods between 30 min to 3 hr, horizontal wavelengths greater than 1000 km) or Medium Scale TIDs (MSTIDs, horizontal speeds between 100 to 250 m s^{-1}, periods between 15 min to 1 hr, and horizontal wavelengths of several hundred km) (e.g., Francis, 1975; Georges, 1968; Ogawa et al., 1987). LSTIDs are typically associated with AGWs generated by Joule heating and particle precipitation from auroral zone disturbances (Hunsucker, 1982; Lyons et al., 2019). These AGWs may propagate equatorward for long distances, transporting energy from the auroral zone to middle and low latitudes (Richmond, 1979) and can even reach the opposite hemisphere (Zakharenkova et al., 2016).

Since first reported by Munro (1948), TIDs have been studied using many different techniques. These include ionosondes (e.g., Galushko et al., 1998, 2003; Altadill et al., 2020), incoherent scatter radars (e.g., Thome, 1964; Kirchengast et al., 1996; Nicolls & Heinselman, 2007; S.-R. Zhang et al., 2021), HF Doppler radars (e.g., Samson et al., 1989, 1990; Bristow et al., 1994; Frissell, Baker, et al., 2014; Frissell et al., 2016), broadcast AM Doppler receivers (Chilcote et al., 2015), global navigation satellite system (GNSS) total electron content (TEC) receivers (e.g., Tsugawa et al., 2007; Zakharenkova et al., 2016; Dinsmore et al., 2021), and airglow imagers (e.g. Mendillo et al., 1997; Otsuka et al., 2004; Ogawa et al., 2009). Each of these different techniques provides a unique and complementary view into understanding the nature of TIDs.

In addition to their scientific value, TIDs are of interest technologically due to their impact on high frequency (HF, 3-30 MHz) terrestrial communications systems. The time-dependent variations in ionospheric electron density associated with TIDs cause a focusing and de-focusing of ionospherically refracted HF radio signals (Samson et al., 1990; Bristow et al., 1994; Frissell, Baker, et al., 2014). These effects can manifest as quasi-periodic fading and enhancements of HF communications signals. Work by the Ham Radio Science Citizen Investigation (HamSCI; hamsci.org) collective have demonstrated that data collected by global-scale, automated HF receiving systems built and operated voluntarily by amateur (ham) radio operators can be used for both scientific study of ionospheric phenomena and as a way to assess ionospheric impacts on real communications systems. This work includes the impacts of solar flares and geomagnetic storms (Frissell, Miller, et al., 2014; Frissell et al., 2019), total solar eclipses (Frissell et al., 2018), and plasma cutoff and single-mode fading (Perry et al., 2018).

In this paper, we present the first observations of LSTIDs in the ionosphere through data collected from the Reverse Beacon Network (RBN), Weak Signal Propagation Reporter Network (WSPRNet), and PSKReporter amateur radio networks. These observations are compared to Blackstone Super Dual Auroral Radar Network (SuperDARN) radar and Global Navigation Satellite System (GNSS) differential Total Electron Content (TEC) observations. Enhancements of the SuperMAG Electrojet (SME) Index and electron densities observed by the Poker Flat Incoherent Scatter Radar (ISR) prior to TID observation suggest auroral activity as the main driver for the observed LSTIDs.

2 Datasets and Methodology

2.1 Amateur Radio

Amateur radio operators are communications hobbyists licensed to transmit on amateur radio frequencies. Radio signals that occur in the high frequency (HF, 3–30 MHz) bands can be refracted back to Earth by the ionosphere, thereby enabling long-distance, over-the-horizon communications. Variability in received signals may be related back to the variations in the ionospheric state. Amateur radio observations have been previously used to show the impacts of solar flares and geomagnetic storms (Frissell, Miller, et al., 2014; Frissell et al., 2019), and also to study the impact of a total solar eclipse (Frissell et al., 2018).

In this paper, we use observations from the RBN (Sinanis et al., 2022), PSKReporter (Gladstone, 2022), and WSPRNet (Walker, 2022) amateur radio networks to study LSTIDs. Each of these networks consists of geographically distributed automated receiving stations that are able to identify and log Morse code and/or digital amateur radio transmissions. Each observed radio transmission is referred to as a "spot" that includes the observation time, frequency, call signs of the transmitter and receiver, and sometimes the transmitter and receiver locations as reported by the radio operator. When station location is not provided, it is determined by looking up the station's licensed callsign in the *HamCall Database* (2022).

2.2 SuperDARN

The Super Dual Auroral Radar Network (SuperDARN) is a global network of coherent-scatter HF Doppler radars that operates between 8 and 20 MHz (Greenwald et al., 1995; Chisham et al., 2007; Nishitani et al., 2019). Although SuperDARN is primarily designed to study ionospheric convection by measuring the Doppler velocity of field aligned ionospheric irregularities, it also routinely observes ground scatter. Ground scatter occurs when radar signals undergo ionospheric refraction back to Earth, reflect off the ground, and then return back to the radar via an ionospheric path. Although the radar returns are from ground reflections, ground scatter can still be used for ionospheric study because the ionosphere will modulate the signals as they propagate through the medium.

Samson et al. (1990); Bristow et al. (1994); Frissell, Baker, et al. (2014) and Frissell et al. (2016) have shown that TIDs moving through the field of view of a SuperDARN radar focus and de-focus the radar rays such that the ground scatter range and signal-to-noise ratio (SNR) vary with the period of the TID. In many ways, SuperDARN ground scatter observations are analogous to amateur radio HF communication links. In both cases, HF radio signals are modulated by the ionosphere before being returned to Earth. Therefore, TIDs have the potential to affect amateur radio HF communications range and SNR in a manner similar to SuperDARN ground scatter observations.

2.3 GNSS Total Electron Content

Dual-frequency Global Navigation Satellite System (GNSS) receiver measurements are now routinely used to measure the Total Electron Content (TEC) in a column between a ground receiver and a satellite in space by measuring the phase difference between the two signals (Coster et al., 1990, 1992). In this paper, we use GNSS TEC data from the CONUS region processed according to the algorithms by Rideout and Coster (2006) and Vierinen et al. (2016). Using a similar approach as Coster et al. (2017), S.-R. Zhang et al. (2017), and S. Zhang et al. (2019), we use a differential TEC (dTEC) analysis rather than absolute TEC to observe the TIDs. In this approach, dTEC values were calculated by subtracting a background TEC variation computed with a low-pass Savitzky-Golay filter (Savitzky & Golay, 1964) using successive windows of 60 min length. Only GNSS satellite-to-ground ray paths with elevations $\geq 30°$ were used.

2.4 Geomagnetic and Auroral Measurements

We use the SuperMAG electrojet (SME) index and Poker Flat Incoherent Scatter Radar (PFISR) observations to quantify possible driving of LSTIDs from auroral sources. SuperMAG is an international collaboration of institutions that combines the observations from over 200 ground-based magnetometers (Gjerloev, 2012). To observe auroral electrojet intensifications, we use the SuperMAG-derived SME index. This value is calculated using data from all available magnetometers between 40°N and 80°N magnetic latitude. Over this range, $\sim$110 stations are available, providing sufficient sampling density to allow for the geographic localization of SME intensifications (Newell & Gjerloev, 2011a, 2011b). The SME index is comparable to the traditional auroral electrojet (AE) index derived by Davis and Sugiura (1966). We employ the SME index because the AE index is derived from only 12 magnetometer stations, making geographic localization of AE enhancements difficult.

PFISR is located near Fairbanks, Alaska (Geographic: 65.13°N, 147.47°W; Magnetic: 65.3°N, 92.1°W). Magnetic midnight occurs at $\sim$UT$-$9.8 hours. For the interval of interest, two radar modes were used: GPSAC5 and IPY27. The GPSAC5 mode is comprised of alternating code observations providing sufficient range resolution to measure E-region electron density (Lehtinen & Häggström, 1987). The IPY27 mode is a low duty cycle background mode composed of both alternating code and uncoded (long) pulse observations. The long pulse observations in the F-region are further processed to estimate the electric field vector using the methodology described by Heinselman and Nicolls (2008). The GPS mode and the IPY27 mode were integrated to 1 minute and 5 minute resolution, respectively.

Electron density observations spanning the interval of interest are provided by the high range resolution alternating code data. For this study, we use the electric field observations, which are limited to the IPY mode observations only, to quantify the passive energy deposition rate, $Q(z) = \sigma_P(z)E^2$, where $\sigma_P(z)$ corresponds to the altitude resolved Pedersen conductivity. More details regarding how the passive energy deposition rate was calculated using PFISR observations can be found in Zhan et al. (2021). The passive energy deposition rate is a proxy for the Joule heating rate, although it excludes the effects from the neutral winds.

3 Observations

3.1 LSTID Observations

Figures 1a and 1b show combined 14 MHz observations from the RBN, PSKReporter, and WSPRNet networks on 3 Nov 2017 for the period of 1200–2359 UT for transmitter-receiver (TX-RX) pairs with great circle distances < 3000 km (to avoid multi-hop situations). This event was selected by making daily summary plots of amateur radio data in a format similar to Figures 1a and 1b and identifying a period with clear LSTID signatures. Figure 1a shows a map of the distribution of TX-RX midpoints of communications observed over the continental United States (CONUS). TX-RX midpoints are calculated based on the assumption that ionospheric refraction occurs at the half-way point between the two stations. Figure 1b presents a time series showing the TX-RX distance for the number of 14 MHz amateur radio spots in 2 min by 25 km bins. The bottom edge of the green-yellow region shows the communications skip focusing distance varying with time, especially between 13 and 18 UT. This skip-distance variation is highlighted by red dots overlaid on the data, which shows a manually-fit fiducial sinusoid with a 2.5 hr period centered around 1050 km range with a 150 km amplitude. A version of this figure without the overlaid sinusoid is presented in Figure 4e.

Figures 1c and 1d show observations from the Blackstone, Virginia (BKS) SuperDARN radar in a format comparable to the amateur radio observations of Figures 1a and 1b. Figure 1c shows the location of the BKS radar and its field-of-view (FOV). Comparison of Figure 1c with Figure 1a reveals that BKS Beam 13 (highlighted in red) looks northwest over a region of dense amateur radio spot coverage. Figure 1d shows power parameter observations from BKS Beam 13. The radar transmit frequency ranged between 10.802 – 11.736 MHz during this time. The scatter is predominantly ground scatter, which is analogous to the amateur radio TX-RX communications distances shown in Figure 1b. Large-scale features can be observed that are common to both the amateur radio and SuperDARN observations. Most importantly, skip distance oscillations are observed in the SuperDARN data that match the those observed in the amateur radio data. The large-scale component of these oscillations is highlighted in Figure 1d with a red dotted sinusoid with identical parameters as the sinusoid in Figure 1b. In both Figures 1b and 1d, it is noted that the sinusoid best matches the data at skip distance maximum, and less so at skip distance minimum. This can be attributed to smaller-scale variations consistent with MSTIDs mixing with the LSTID activity.

We next compare the amateur radio and SuperDARN observations with GNSS dTEC measurements. Figure 1e shows a map of CONUS dTEC at 1343 UT, corresponding to the time of the first skip-distance maximum of the sinusoid in Figure 1b. LSTID wavefronts occurred with a southwest to northeast orientation, especially in the central and Eastern portions of the CONUS. 1343 UT corresponds to a negative phase of the LSTIDs over the CONUS, as indicated by dTEC values of $\sim$ -0.2 for a large portion of the map. The black inset box in Figure 1e indicates the region from 30° to 50°N latitude and 70° to 120°W longitude. A time series of the median dTEC values within this region is presented in Figure 1f (blue line). The dotted orange line shows the data filtered with a 2 – 4 hr bandpass filter. Significant wave activity occurred in this time series data, and comparison to amateur radio and SuperDARN observations show a general trend: depressions in median dTEC correspond to increases in skip distance, and vice-versa. The FFT spectral analysis of the median dTEC time series shown in Figure 1g shows that the dominant spectral component of dTEC had a period of 2.4 hr, in excellent agreement with 2.5 hr oscillations measured with the sinusoid fit to the amateur radio and SuperDARN data.

Figure 2 further shows the spatial and temporal relationship between amateur radio and GNSS dTEC LSTID observations. Figure 2a presents the amateur radio data first shown in Figure 1b. The 2.5 hr sinusoid from Figure 1b is overlaid with red dots and the median dTEC values from Figure 1f are overlaid as a solid white line. The dotted sinusoid and the median dTEC values exhibit an anti-correlated relationship. Four times, corresponding with the maxima and minima of the 2.5 hr sinusoid, are identified with vertical dashed lines. Maps of GNSS dTEC observations corresponding to these times are shown in Figures 2b – 2e. Results show an inverse relationship between the amateur radio skip distances observed in Figure 2a and the dTEC measurements in Figures 2b – 2e. Specifically, when maxima in amateur radio skip distances occur at 1343 and 1613 UT, a decrease of ~ 0.20 TECu is observed in the central regions of the maps. Conversely, when minima in amateur radio skip distances occur at 1458 and 1728 UT, an increase of ~ 0.20 TECu is observed. Wavefronts oriented from southwest to northeast can be observed in the dTEC maps. This is most clearly seen in Figure 2d, where a black arrow indicates the estimated horizontal wavelength ($\lambda_h \approx 1680$ km) and propagation azimuth ($\alpha \approx 163°$) of the largest wave feature in the map. Movie versions of Figure 2 showing the full progression of dTEC with time are provided in Supporting Information S1 and S2. Using this movie and the open-source Tracker Video Analysis and Modeling tool (Brown & Cox, 2009), the phase speed of the southeastward propagating LSTID trough between 1300 and 1400 UT was estimated to be $\sim$1220 km hr^{-1}.

In order to estimate the phase speed of the LSTIDs in the amateur radio data, Figure 3 shows time series of latitudinal and longitudinal data slices plotted using a saturated filled contour from 1400 to 1800 UT. This time range is centered around the 1618 UT skip distance maximum identified in Figure 2a. The top four rows show 1° latitudinal slices that range from 42° to 38°N and extend from 88° to 74°W longitude. The bottom four rows show 2° longitudinal slices that range from 85° to 79°W and extend from 37° to 44°N latitude. Red arrows indicate the time of the skip distance maxima manually identified in each time series plot. The arrows in the latitudinal slices indicate a steady forward progression in time from the slice centered at 41.5°N to the one centered at 39.5°N, consistent with a north-to-south propagating LSTID. Using a linear regression of distance traveled versus time, the north-to-south phase velocity was estimated to be $\sim$1206 km hr^{-1}. Note that the skip distance maximum in the 38.5°N slice appeared to move backwards in time. We ascribe this non-coherent behavior (compared to higher latitude bins) to the multi-dimensional complexity of the wave field the radio signals propagated through at that time. The red arrows in the longitudinal slices (Figure 2b) show almost no progression with time, which is consistent with a predominantly north-south propagating LSTID that has east-west oriented wavefronts spanning the entire longitudinal observational range.

3.2 Geomagnetic Conditions and Auroral Zone Drivers

Figure 4 shows evidence of auroral zone activity preceding the midlatitude observation of LSTIDs by amateur radio. Signatures of two auroral electrojet enhancements can be seen in Figure 4a, where the SME index first peaked to $\sim$500 nT between 10 and 12 UT, and then subsequently increased to $\sim$700 nT between 12 and 13 UT. Figure 4b presents the regional SME index, which indicates that these enhancements occurred within the 22 – 04 magnetic local time (MLT) sector. This occurs during the recovery phase of a minor geomagnetic storm with Kp $\leq$ 3+ and minimum Sym-H ≈ -30 nT at 00

UT. Figure 4c shows that these electrojet surges were associated with electron density enhancements from 90 to 150 km altitude as measured by PFISR, whose observation point migrated from 2125 MLT at 8 UT to 0230 MLT at 13 UT. These electron density enhancements were also associated with significant Joule heating measured by PFISR at these same altitudes, as shown in Figure 4d. Figure 4e again presents the amateur radio data in a similar format to Figure 1a, now starting at 08 UT. Figure 4e shows that the TIDs are observed at midlatitudes by the amateur radio networks $\sim$2 to 3 hours after the onset of auroral zone activity. Note that no radio spots were observed between 8 and 12 UT because of a lack of 14 MHz radio propagation, due to lower nighttime midlatitude ionospheric electron densities.

The large-scale nature of the observed mid-latitude LSTIDs and their predominantly equatorward propagation suggest that an auroral zone source is likely. We can relate the TID observations to the auroral zone disturbances by estimating the location of the source region using the measurements of LSTID phase speed, propagation azimuth, and timing. To estimate the location of the LSTID source region, we start at the point corresponding to the arrow tail in Figure 2d at the top of the LSTID observation region (44°N, 93°W). We then project backwards from the 163° propagation azimuth at the phase speeds determined using the amateur radio and GNSS dTEC data. A low estimate using a 2 hr propagation time and 1100 km hr^{-1} speed places the source region at geographic (62°N, 105°W) and magnetic (70°N, 43°W, 0239 MLT). A high estimate using a 3 hr propagation time and 1300 km hr^{-1} speed places the source region at geographic (76°N, 132°W) and magnetic (77°N, 87°W, 2341 MLT). Both of these estimates place the source region in areas consistent with the auroral electrojet enhancement observed using SME index and the Joule heating enhancement observed using the PFISR radar. This supports the hypothesis that LSTIDs are generated by AGWs generated by auroral zone Joule heating and particle precipitation (e.g., Hunsucker, 1982; Lyons et al., 2019).

4 Discussion

We used data from large-scale, automated, crowd sourced amateur radio networks to observe the effects of LSTIDs on 14 MHz HF communications paths over the continental United States. These observations are in excellent agreement with skip-distance measurements made by the Blackstone, VA SuperDARN radar and dTEC measurements made by ground-based GNSS receivers. Observations of LSTIDs by these amateur radio networks are significant for two reasons. First, these observations demonstrate a novel technique for the scientific study and characterization of LSTIDs. The RBN, WSPRNet, and PSKReporter amateur radio networks have global-scale data that extends over an entire solar cycle back to 2008 and simultaneously observes multiple frequency bands from 1.8 to 30 MHz. These datasets have the potential to complement and extend existing professional instrumentation networks both in geographic and spectral extent. The results here indicate that these datasets are appropriate for statistical searches of LSTIDs similar to Frissell et al. (2016), and such analyses can provide further understanding of the nature of LSTIDs and their connection to space and the neutral atmosphere. Secondly, this new technique now allows LSTID impacts on actual HF communications systems to be assessed and directly related to measurements made by professional scientific instrumentation. This has the potential to enable the future development of methodologies to better understand and potentially predict the impacts of space weather and the atmosphere on HF communications systems.

While we have highlighted the agreement of the amateur radio, SuperDARN, and GNSS dTEC TID observations, it is also important to note some of the differences and recognize that each technique does in fact provide a unique view of the ionosphere. Amateur radio and SuperDARN both sense TIDs through bottomside oblique HF ionospheric sounding and therefore have similar measurements. Still, the amateur radio observations are able to show a continental-scale ionospheric behavior that may not be appreciated with SuperDARN radars. Conversely, SuperDARN is able to better resolve fine-scale TID structures than the amateur radio technique.

It is also not reasonable to assume a strict one-to-one mapping of TIDs observed with the bottomside HF sounding techniques and the GNSS dTEC technique. GNSS TEC is a height integrated measurement that is not guaranteed to be sensitive to ionospheric structures at the same altitudes as the HF systems. This is evidenced in the backward phase progression seen at 38.5°N in Figure 3. This dichotomy has been reported in other studies. Chilcote et al. (2015) showed, for example, that TIDs detected using Doppler shift observations of AM broadcast signals propagated in the opposite direction of TIDs detected with GNSS dTEC. In general, we emphasize that different techniques may be useful for extracting greater information through collective multi-technique study of a single event, and also emphasize that each technique may provide unique information in its own right.

This paper demonstrates only the first example of using amateur radio networks to study LSTIDs. Future work includes automating amateur radio LSTID detection, improving the ability to localize LSTID measurements and estimate propagation direction, conducting statistical studies, and working towards the development of methods to better resolve smaller-scale features such as MSTIDs. There are also important implications for ionospheric citizen science, as the HamSCI Personal Space Weather Station project (Collins et al., 2021) will be capable of contributing to both the WSPRNet and PSKReporter datasets. We recognize that the amateur transmissions employed here are not guaranteed to be regular or continuous. Therefore, certain challenges exist in extending this technique to a larger statistical study. However, these data gaps are similar in nature to gaps due to propagation conditions in the SuperDARN data set and could be addressed in a manner similar to Frissell, Baker, et al. (2014) and Frissell et al. (2016). Additionally, a manual LSTID climatology for 2017 by Sanchez et al. (2021) shows that sufficiently regular amateur radio observations exist to support statistical studies, especially over North America and Europe.

5 Summary

We demonstrated a novel method for observing Large Scale Traveling Ionospheric Disturbances (LSTIDs) using high frequency (HF) amateur radio reporting networks, including the Reverse Beacon Network (RBN), Weak Signal Propagation Reporter Network (WSPRNet), and PSKReporter. On 3 Nov 2017, LSTID signatures were observed simultaneously over the continental United States in amateur radio, SuperDARN HF radar, and GNSS Total Electron Content with a period of $\sim$2.5 hr, propagation azimuth of $\sim$163°, horizontal wavelength of $\sim$1680 km, and phase speed of $\sim$1200 km hr^{-1}. SuperMAG SME index enhancements and Poker Flat Incoherent Scatter Radar measurements suggest the LSTIDs were driven by auroral electrojet intensifications and Joule heating. This novel measurement technique has applications in future scientific studies and for assessing the impact of LSTIDs on HF communications.

Acknowledgments

The authors gratefully acknowledge the support of United States National Science Foundation (NSF) Grants AGS-2045755 and AGS-2002278 and NASA Grants 80NSSC21K0002 and 80NSSC21K1772. We are especially grateful to the amateur radio community who voluntarily produced and provided the HF radio observations used in this presentation, especially the operators of the reversebeacon.net, wsprnet.org, pskreporter.info, and hamcall.net. Blackstone SuperDARN data are made available with support from NSF AGS-1935110. This material is based upon work supported by the Poker Flat Incoherent Scatter Radar which is a major facility funded by the NSF through cooperative agreement AGS-1840962 to SRI

International. Algorithms used to calculate the electric field and Joule heating rates were developed under NSF AGS-1853408 and AGS-1552269. GNSS TEC data products and access through the Madrigal distributed data system are provided to the community by the Massachusetts Institute of Technology under support from NSF grant AGS-1952737. Individual contributors of GNSS data are listed in the Open Research section. We gratefully acknowledge the SuperMAG collaborators (https://supermag.jhuapl.edu/info/?page=acknowledgement) who contributed to the SuperMAG database (Gjerloev, 2012) and the SuperMAG SME(r) indices (Newell & Gjerloev, 2011a, 2011b). NAF thanks Rachel Frissell, Bill Liles, Ethan Miller, and Dev Raj Joshi for helpful discussions.

Open Research

Amateur radio data from the Reverse Beacon Network (RBN), Weak Signal Propagation Reporter Network (WSPRNet), and PSKReporter used in this paper has been aggregated and deposited into a Zenodo repository (Frissell & Engelke, 2021). SuperDARN data used in this paper is available from Ruohoniemi et al. (2022) and can be visualized with the open-source pyDARN toolkit (Schmidt et al., 2021). SuperMAG data are available from SuperMAG database (*SuperMAG Database*, 2022). The Kp and SymH indices were accessed through the OMNI database at the NASA Space Physics Data Facility (*NASA CDAWeb*, 2022). We acknowledge the use of the Free Open Source Software projects used in this analysis: Ubuntu Linux, python (van Rossum, 1995), matplotlib (Hunter, 2007), NumPy (Oliphant, 2007), SciPy (Jones et al., 2001), pandas (McKinney, 2010), xarray (Hoyer & Hamman, 2017), iPython (Pérez & Granger, 2007), and others (e.g., Millman & Aivazis, 2011).

The GNSS TEC and Poker Flat Incoherent Scatter Radar data are available for download from the Madrigal database system maintained by Massachusetts Institute of Technology's Haystack Observatory (*CEDAR Madrigal Database*, 2022). Data for the TEC processing is provided from the following organizations: UNAVCO, Scripps Orbit and Permanent Array Center, Institut Geographique National, France, International GNSS Service, The Crustal Dynamics Data Information System (CDDIS), National Geodetic Survey, Instituto Brasileiro de Geografia e Estatística, RAMSAC CORS of Instituto Geográfico Nacional de la República Argentina, Arecibo Observatory, Low-Latitude Ionospheric Sensor Network (LISN), Topcon Positioning Systems, Inc., Canadian High Arctic Ionospheric Network, Institute of Geology and Geophysics, Chinese Academy of Sciences, China Meteorology Administration, Centro di Ricerche Sismologiche, Système d'Observation du Niveau des Eaux Littorales (SONEL), RENAG : REseau NAtional GPS permanent, GeoNet - the official source of geological hazard information for New Zealand, GNSS Reference Networks, Finnish Meteorological Institute, SWEPOS - Sweden, Hartebeesthoek Radio Astronomy Observatory, TrigNet Web Application, South Africa, Australian Space Weather Services, RETE INTEGRATA NAZIONALE GPS, Estonian Land Board, Virginia Tech Center for Space Science and Engineering Research, and Korea Astronomy and Space Science Institute.

References

Altadill, D., Segarra, A., Blanch, E., Juan, J. M., Paznukhov, V. V., Buresova, D., . . . Belehaki, A. (2020). A method for real-time identification and tracking of traveling ionospheric disturbances using ionosonde data: first results. *Journal of Space Weather and Space Climate*, *10*, 2. doi: 10.1051/SWSC/2019042

Bristow, W. A., Greenwald, R. A., & Samson, J. C. (1994). Identification of High-Latitude Acoustic Gravity Wave Sources Using the Goose Bay HF Radar. *J. Geophys. Res.*, *99*(A1), 319–331. Retrieved from `http://dx.doi.org/10.1029/93JA01470` doi: 10.1029/93JA01470

Brown, D., & Cox, A. J. (2009). Innovative Uses of Video Analysis. *The Physics Teacher*, *47*(3), 145. Retrieved from `https://physlets.org/tracker/` doi: 10.1119/1.3081296

CEDAR Madrigal Database. (2022). Retrieved from `http://cedar.openmadrigal.org/`

Chilcote, M., LaBelle, J., Lind, F. D., Coster, A. J., Miller, E. S., Galkin, I. A., & Weatherwax, A. T. (2015). Detection of traveling ionospheric disturbances by medium-frequency Doppler sounding using AM radio transmissions. *Radio Science*, *50*(3), 249–263. doi: 10.1002/2014RS005617

Chisham, G., Lester, M., Milan, S. E., Freeman, M. P., Bristow, W. A., Grocott, A., . . . Walker, A. D. M. (2007). A decade of the Super Dual Auroral Radar Network (SuperDARN): scientific achievements, new techniques, and future directions. *Surveys in Geophys.*, 33–109. doi: 10.1007/s10712-007-9017-8

Collins, K., Kazdan, D., & Frissell, N. A. (2021). Ham Radio Forms a Planet-Sized Space Weather Sensor Network. *Eos*, *102*. doi: 10.1029/2021eo154389

Coster, A. J., Buonsanto, M., Gaposchkin, E. M., Tetenbaum, D., & Thornton, L. E. (1990). Ionospheric and tropospheric path delay obtained from GPS integrated phase, incoherent scatter and refractometer data and from IRI-86. *Advances in Space Research*, *10*(8), 105–108. doi: 10.1016/0273-1177(90)90194-5

Coster, A. J., Gaposchkin, E. M., & Thornton, L. E. (1992). Real-Time Ionospheric Monitoring System Using GPS. *Navigation*, *39*(2), 191–204. doi: 10.1002/J.2161-4296.1992.TB01874.X

Coster, A. J., Goncharenko, L., Zhang, S.-R., Erickson, P. J., Rideout, W., & Vierinen, J. (2017). GNSS Observations of Ionospheric Variations During the 21 August 2017 Solar Eclipse. *Geophysical Research Letters*. Retrieved from `http://dx.doi.org/10.1002/2017GL075774` doi: 10.1002/2017GL075774

Davis, T. N., & Sugiura, M. (1966). Auroral Electrojet Activity Index {AE} and Its Universal Time Variations. *J. Geophys. Res.*, *71*(3), 785–801. Retrieved from `http://dx.doi.org/10.1029/JZ071i003p00785` doi: 10.1029/JZ071i003p00785

Dinsmore, R., Mathews, J. D., Coster, A., Robinson, R. M., Sarkhel, S., Erickson, P. J., & Urbina, J. (2021). Multi-instrument observations of SCIPS: 1. ISR and GPS TEC results. *Journal of Atmospheric and Solar-Terrestrial Physics*, *213*, 105515. doi: 10.1016/j.jastp.2020.105515

Francis, S. H. (1975). Global propagation of atmospheric gravity waves: A review. *Journal of Atmospheric and Terrestrial Physics*, *37*(6–7), 1011–1054. Retrieved from `http://www.sciencedirect.com/science/article/pii/0021916975900124` doi: http://dx.doi.org/10.1016/0021-9169(75)90012-4

Frissell, N. A., Baker, J. B. H., Ruohoniemi, J. M., Gerrard, A. J., Miller, E. S., Marini, J. P., . . . Bristow, W. A. (2014). Climatology of medium-scale traveling ionospheric disturbances observed by the midlatitude Blackstone SuperDARN radar. *Journal of Geophysical Research: Space Physics*, *119*(9). Retrieved from `http://dx.doi.org/10.1002/2014JA019870` doi: 10.1002/2014JA019870

Frissell, N. A., Baker, J. B. H., Ruohoniemi, J. M., Greenwald, R. A., Gerrard, A. J., Miller, E. S., & West, M. L. (2016). Sources and Characteristics of

Medium Scale Traveling Ionospheric Disturbances Observed by High Frequency Radars in the North American Sector. *Journal of Geophysical Research: Space Physics*. Retrieved from http://dx.doi.org/10.1002/2015JA022168 doi: 10.1002/2015JA022168

Frissell, N. A., & Engelke, W. D. (2021). *Dataset for "First Observations of Large Scale Traveling Ionospheric Disturbances Using Automated Amateur Radio Receiving Networks".* Zenodo. Retrieved from https://doi.org/10.5281/zenodo.5799648 doi: 10.5281/zenodo.5799648

Frissell, N. A., Katz, J. D., Gunning, S. W., Vega, J. S., Gerrard, A. J., Earle, G. D., … Silver, H. W. (2018). Modeling Amateur Radio Soundings of the Ionospheric Response to the 2017 Great American Eclipse. *Geophysical Research Letters*, *45*(10), 4665–4674. Retrieved from https://doi.org/10.1029/2018GL077324 doi: 10.1029/2018GL077324

Frissell, N. A., Miller, E. S., Kaeppler, S., Ceglia, F., Pascoe, D., Sinanis, N., … Shovkoplyas, A. (2014). Ionospheric Sounding Using Real-Time Amateur Radio Reporting Networks. *Space Weather*, *12*(12). doi: http://dx.doi.org/10.1002/2014SW001132

Frissell, N. A., Vega, J. S., Markowitz, E., Gerrard, A. J., Engelke, W. D., Erickson, P. J., … Bortnik, J. (2019). High-Frequency Communications Response to Solar Activity in September 2017 as Observed by Amateur Radio Networks. *Space Weather*, *17*(1), 118–132. doi: 10.1029/2018SW002008

Galushko, V. G., Beley, V. S., Koloskov, A. V., Yampolski, Y. M., Paznukhov, V. V., Reinisch, B. W., … Erickson, P. (2003). Frequency-and-angular HF sounding and ISR diagnostics of TIDs. *Radio Science*, *38*(6), 1102. doi: 10.1029/2002RS002861

Galushko, V. G., Paznukhov, V. V., Yampolski, Y. M., & Foster, J. C. (1998). Incoherent scatter radar observations of AGW/TID events generated by the moving solar terminator. *Annales Geophysicae*, *16*(7), 821–827. Retrieved from http://www.ann-geophys.net/16/821/1998/ doi: 10.1007/s00585-998-0821-3

Georges, T. M. (1968). HF Doppler studies of traveling ionospheric disturbances. *Journal of Atmospheric and Terrestrial Physics*, *30*(5), 735–746. Retrieved from http://www.sciencedirect.com/science/article/pii/S0021916968800297 doi: 10.1016/S0021-9169(68)80029-7

Gjerloev, J. W. (2012, 9). The SuperMAG data processing technique. *Journal of Geophysical Research: Space Physics*, *117*(A9), 9213. doi: 10.1029/2012JA017683

Gladstone, P. (2022). *PSKReporter.* Retrieved from https://pskreporter.info/

Greenwald, R. A., Baker, K. A., Dudeney, J. R., Pinnock, M., Jones, T. B., Thomas, E. C., … Yamagishi, H. (1995). DARN/SuperDARN: A global view of the dynamics of high-latitude convection. *Space Sci. Rev.*, 761–796. doi: https://doi.org/10.1007/BF00751350

HamCall Database. (2022). Retrieved from https://hamcall.net/

Heinselman, C. J., & Nicolls, M. J. (2008). A Bayesian approach to electric field and E-region neutral wind estimation with the Poker Flat Advanced Modular Incoherent Scatter Radar. *Radio Science*, *43*(5), n/a-n/a. doi: 10.1029/2007RS003805

Hines, C. O. (1960). Internal Atmospheric Gravity Waves at Ionospheric Heights. *Canadian Journal of Physics*, *38*(11), 1441–1481. Retrieved from http://www.nrcresearchpress.com/doi/abs/10.1139/p60-150 doi: 10.1139/p60-150

Hoyer, S., & Hamman, J. (2017). xarray: {N-D} labeled arrays and datasets in {Python}. *Journal of Open Research Software*, *5*(1). Retrieved from http://doi.org/10.5334/jors.148 doi: 10.5334/jors.148

Hunsucker, R. D. (1982). Atmospheric gravity waves generated in the high-latitude ionosphere: A review. *Reviews of Geophysics*, *20*(2), 293–315.

Retrieved from http://dx.doi.org/10.1029/RG020i002p00293 doi: 10.1029/RG020i002p00293

Hunter, J. D. (2007). Matplotlib: A 2D graphics environment. *Computing In Science & Engineering*, *9*(3), 90–95. doi: 10.1109/MCSE.2007.55

Jones, E., Oliphant, T., Peterson, P., & others. (2001). *SciPy: Open source scientific tools for Python.* Retrieved from http://www.scipy.org/

Kirchengast, G., Hocke, K., & Schlegel, K. (1996). The gravity wave-TID relationship: insight via theoretical model—EISCAT data comparison. *Journal of Atmospheric and Terrestrial Physics*, *58*(1–4), 233–243. Retrieved from http://www.sciencedirect.com/science/article/pii/0021916995000321 doi: http://dx.doi.org/10.1016/0021-9169(95)00032-1

Lehtinen, M. S., & Häggström, I. (1987). A new modulation principle for incoherent scatter measurements. *Radio Science*, *22*(4), 625–634. doi: 10.1029/RS022I004P00625

Lyons, L. R., Nishimura, Y., Zhang, S., Coster, A. J., Bhatt, A., Kendall, E., & Deng, Y. (2019). Identification of Auroral Zone Activity Driving Large-Scale Traveling Ionospheric Disturbances. *Journal of Geophysical Research: Space Physics*, *124*(1), 700–714. doi: 10.1029/2018JA025980

McKinney, W. (2010). Data Structures for Statistical Computing in Python. In S. van der Walt & J. Millman (Eds.), *Proceedings of the 9th python in science conference* (pp. 51–56).

Mendillo, M., Baumgardner, J., Nottingham, D., Aarons, J., Reinisch, B., Scali, J., & Kelley, M. (1997). Investigations of thermospheric-ionospheric dynamics with 6300-Å images from the Arecibo Observatory. *Journal of Geophysical Research: Space Physics*, *102*(A4), 7331–7343. Retrieved from http://dx.doi.org/10.1029/96JA02786 doi: 10.1029/96JA02786

Millman, K. J., & Aivazis, M. (2011). Python for Scientists and Engineers. *Computing in Science & Engineering*, *13*(2), 9–12. doi: 10.1109/MCSE.2011.36

Munro, G. H. (1948). Short-Period Changes in the F Region of the Ionosphere. *Nature*, *162*(4127), 886–887. doi: 10.1038/162886a0

NASA CDAWeb. (2022). Retrieved from https://cdaweb.gsfc.nasa.gov/

Newell, P. T., & Gjerloev, J. W. (2011a). Evaluation of SuperMAG auroral electrojet indices as indicators of substorms and auroral power. *Journal of Geophysical Research: Space Physics*, *116*(A12). doi: 10.1029/2011JA016779

Newell, P. T., & Gjerloev, J. W. (2011b). Substorm and magnetosphere characteristic scales inferred from the SuperMAG auroral electrojet indices. *Journal of Geophysical Research: Space Physics*, *116*(A12), 12232. doi: 10.1029/2011JA016936

Nicolls, M. J., & Heinselman, C. J. (2007). Three-dimensional measurements of traveling ionospheric disturbances with the Poker Flat Incoherent Scatter Radar. *Geophysical Research Letters*, *34*(21). Retrieved from http://dx.doi.org/10.1029/2007GL031506 doi: 10.1029/2007GL031506

Nishitani, N., Ruohoniemi, J. M., Lester, M., Baker, J. B. H., Koustov, A. V., Shepherd, S. G., … Kikuchi, T. (2019). Review of the accomplishments of mid-latitude Super Dual Auroral Radar Network (SuperDARN) HF radars. *Progress in Earth and Planetary Science*, *6*(1), 27. Retrieved from https://progearthplanetsci.springeropen.com/articles/10.1186/s40645-019-0270-5 doi: 10.1186/s40645-019-0270-5

Ogawa, T., Igarashi, K., Aikyo, K., & Maeno, H. (1987). NNSS satellite observations of medium-scale traveling ionospheric disturbances at southern high-latitudes. *Journal of Geomagnetism and Geoelectricity*, *39*, 709–721.

Ogawa, T., Nishitani, N., Otsuka, Y., Shiokawa, K., Tsugawa, T., & Hosokawa, K. (2009). Medium-scale traveling ionospheric disturbances observed with the SuperDARN Hokkaido radar, all-sky imager, and GPS network and their relation to concurrent sporadic E irregularities. *Journal of Geophysical Research:*

Space Physics, *114*(A3). Retrieved from http://dx.doi.org/10.1029/2008JA013893 doi: 10.1029/2008JA013893

Oliphant, T. E. (2007). Python for Scientific Computing. *Computing in Science Engineering*, *9*(3), 10–20. doi: 10.1109/MCSE.2007.58

Otsuka, Y., Shiokawa, K., Ogawa, T., & Wilkinson, P. (2004). Geomagnetic conjugate observations of medium-scale traveling ionospheric disturbances at midlatitude using all-sky airglow imagers. *Geophysical Research Letters*, *31*(15). Retrieved from http://dx.doi.org/10.1029/2004GL020262 doi: 10.1029/2004GL020262

Pérez, F., & Granger, B. E. (2007). IPython: a System for Interactive Scientific Computing. *Computing in Science and Engineering*, *9*(3), 21–29. Retrieved from http://ipython.org doi: 10.1109/MCSE.2007.53

Perry, G. W., Frissell, N. A., Miller, E. S., Moses, M., Shovkoplyas, A., Howarth, A. D., & Yau, A. W. (2018). Citizen Radio Science: An Analysis of Amateur Radio Transmissions With e-POP RRI. *Radio Science*, *53*(8), 933–947. Retrieved from https://agupubs.onlinelibrary.wiley.com/doi/abs/10.1029/2017RS006496 doi: 10.1029/2017RS006496

Richmond, A. D. (1979). Large-amplitude gravity wave energy production and dissipation in the thermosphere. *Journal of Geophysical Research: Space Physics*, *84*(A5), 1880–1890. doi: 10.1029/JA084IA05P01880

Rideout, W., & Coster, A. (2006). Automated GPS processing for global total electron content data. *GPS Solutions*, *10*(3), 219–228. Retrieved from http://dx.doi.org/10.1007/s10291-006-0029-5 doi: 10.1007/s10291-006-0029-5

Ruohoniemi, J. M., Baker, J. B. H., & Sterne, K. (2022). *Virginia Tech SuperDARN Website.* Retrieved from http://vt.superdarn.org/

Samson, J. C., Greenwald, R. A., Ruohoniemi, J. M., & Baker, K. B. (1989). High-frequency radar observations of atmospheric gravity waves in the high-latitude ionosphere. *Geophys. Res. Lett.*, *16*(8), 875–878. Retrieved from http://dx.doi.org/10.1029/GL016i008p00875 doi: 10.1029/GL016i008p00875

Samson, J. C., Greenwald, R. A., Ruohoniemi, J. M., Frey, A., & Baker, K. B. (1990). Goose Bay Radar Observations of Earth-Reflected, Atmospheric Gravity Waves in the High-Latitude Ionosphere. *J. Geophys. Res.*, *95*(A6), 7693–7709. Retrieved from http://dx.doi.org/10.1029/JA095iA06p07693 doi: 10.1029/JA095iA06p07693

Sanchez, D. F., Frissell, N. A., Perry, G., Harvey, L., Engelke, W. D., Coster, A. J., ... Baker, J. B. H. (2021). Climatology of Traveling Ionospheric Disturbances Observed by HamSCI Amateur Radio with Connections to Geospace and Neutral Atmospheric Sources. In *American geophysical union fall meeting.* New Orleans, LA. Retrieved from https://agu2021fallmeeting-agu.ipostersessions.com/?s=02-7A-CD-78-5C-8E-89-DE-07-4F-08-3C-F8-B3-FD-E6

Savitzky, A., & Golay, M. J. E. (1964). Smoothing and Differentiation of Data by Simplified Least Squares Procedures. *Analytical Chemistry*, *36*(8), 1627–1639. doi: 10.1021/AC60214A047

Schmidt, M. T., Tholley, F., Martin, C. J., Billett, D. D., Bland, E. C., Coyle, S., ... Roberston, C. R. (2021). *SuperDARN/pydarn: pyDARN v2.2.1.* Zenodo. Retrieved from https://doi.org/10.5281/zenodo.5762322 doi: 10.5281/zenodo.5762322

Sinanis, N., Pascoe, D., Glenn, M., Smith, P., Ceglia, F., & Williams, D. (2022). *Reverse Beacon Network.* Retrieved from http://www.reversebeacon.net/

SuperMAG Database. (2022). Retrieved from https://supermag.jhuapl.edu/

Thome, G. D. (1964). Incoherent scatter observations of traveling ionospheric disturbances. *Journal of Geophysical Research*, *69*(19), 4047–4049. Retrieved from http://dx.doi.org/10.1029/JZ069i019p04047 doi: 10.1029/JZ069i019p04047

Tsugawa, T., Otsuka, Y., Coster, A. J., & Saito, A. (2007). Medium-scale traveling ionospheric disturbances detected with dense and wide TEC maps over North America. *Geophysical Research Letters*, *34*(22). doi: 10.1029/2007GL031663

van Rossum, G. (1995). *Python tutorial* (Tech. Rep. No. CS-R9526). Amsterdam: Centrum voor Wiskunde en Informatica (CWI).

Vierinen, J., Coster, A. J., Rideout, W. C., Erickson, P. J., & Norberg, J. (2016). Statistical framework for estimating GNSS bias. *Atmospheric Measurement Techniques*, *9*(3), 1303–1312. doi: 10.5194/amt-9-1303-2016

Walker, B. (2022). *WSPRNet.* Retrieved from `https://www.wsprnet.org/`

Zakharenkova, I., Astafyeva, E., & Cherniak, I. (2016). GPS and GLONASS observations of large-scale traveling ionospheric disturbances during the 2015 St. Patrick's Day storm. *Journal of Geophysical Research: Space Physics*, *121*(12), 138–12. doi: 10.1002/2016JA023332

Zhan, W., Kaeppler, S. R., Larsen, M. F., Reimer, A., & Varney, R. (2021). An Investigation of Auroral E Region Energy Exchange Using Poker Flat Incoherent Scatter Radar Observations During Fall Equinox Conditions. *Journal of Geophysical Research: Space Physics*, *126*(10), e2021JA029371. doi: 10.1029/2021JA029371

Zhang, S., Coster, A. J., Erickson, P. J., Goncharenko, L. P., Rideout, W., & Vierinen, J. (2019). Traveling Ionospheric Disturbances and Ionospheric Perturbations Associated With Solar Flares in September 2017. *Journal of Geophysical Research: Space Physics*, *124*(7), 5894–5917. Retrieved from `https://onlinelibrary.wiley.com/doi/abs/10.1029/2019JA026585` doi: 10.1029/2019JA026585

Zhang, S.-R., Erickson, P. J., Gasque, L. C., Aa, E., Rideout, W., Vierinen, J., . . . Coster, A. J. (2021). Electrified Postsunrise Ionospheric Perturbations at Millstone Hill. *Geophysical Research Letters*, *48*(18), e2021GL095151. doi: 10.1029/2021GL095151

Zhang, S.-R., Erickson, P. J., Goncharenko, L. P., Coster, A. J., Rideout, W., & Vierinen, J. (2017). Ionospheric Bow Waves and Perturbations Induced by the 21 August 2017 Solar Eclipse. *Geophysical Research Letters*, *44*(24), 067–12. doi: 10.1002/2017GL076054

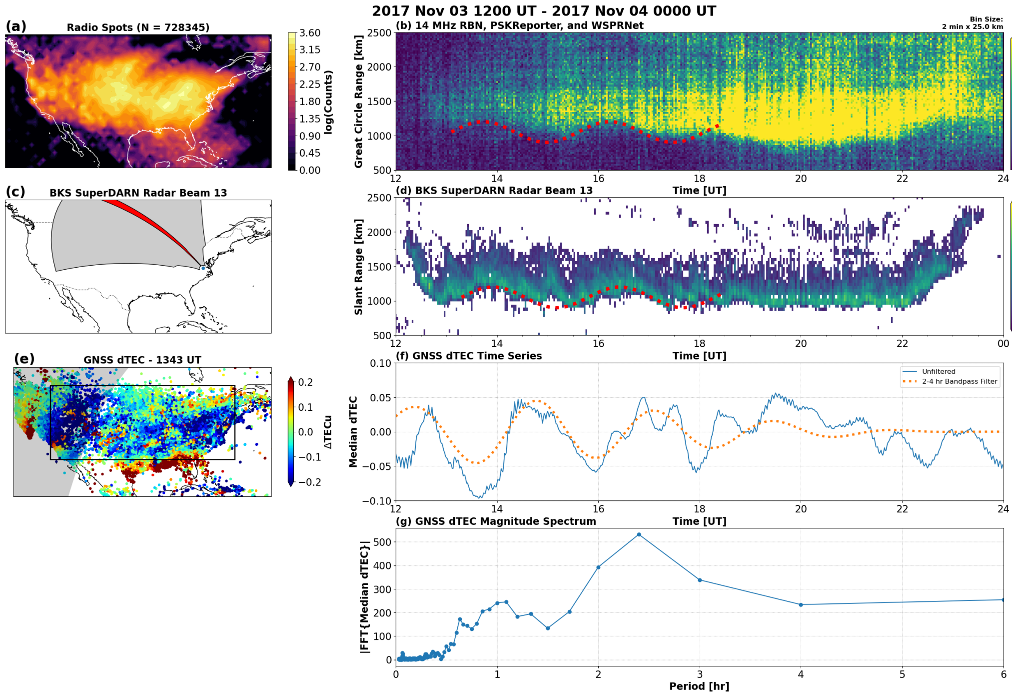

Figure 1. LSTIDs observed using amateur radio networks, the BKS SuperDARN radar, and GNSS dTEC. (a) Geographic distribution of TX-RX midpoints of amateur radio communications observed over the continental United States on 3 Nov 2017 from 1200-2359 UT. (b) Time series showing the TX-RX distance for 14 MHz amateur radio spots in 2 min by 25 km bins. (c) Location and FOV of the BKS SuperDARN radar; Beam 13 is highlighted in red. (d) Ground scatter power observations of BKS Beam 13 with ∼11 MHz transmit frequency. (e) GNSS dTEC measurements at 1343 UT. (f) Time series (blue line) of GNSS dTEC median values calculated from measurements in the black box region in (e). Dotted orange line shows data filtered with a 2 – 4 hr bandpass filter. (g) FFT Magnitude spectrum of the unfiltered data in (f). Red dots overlaid on (b) and (d) show a sinusoidal 2.5 hr oscillation in skip distance common to both the amateur radio and SuperDARN measurements.

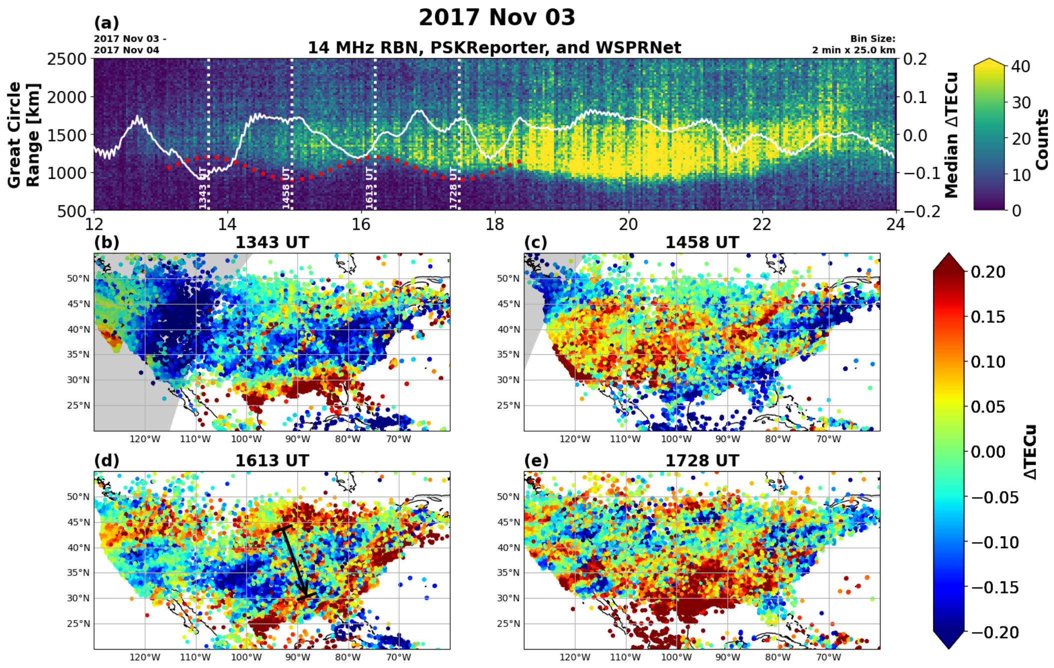

Figure 2. Amateur radio and GNSS dTEC observations of the 3 Nov 2017 LSTIDs. (a) CONUS amateur radio observations in the same format as Figure 1b. The red dashed sinusoid highlights the 2.5 hour skip distance oscillation; the white solid line shows the median dTEC values first presented in Figure 1f. Vertical white dashed lines indicate sinusoid maxima and minima times. (b – e) GNSS dTEC maps corresponding to the skip distance maxima and minima times indicated in (a). A black arrow is drawn on (d) indicating the estimated horizontal wavelength ($\lambda_h \approx 1680$ km) and direction of travel ($\alpha \approx 163°$) of the GNSS LSTIDs corresponding with the amateur radio LSTIDs. A decrease of ∼0.2 TECu is observed in the central region of the maps during skip distance maxima, while an increase of ∼0.2 TECu is observed during skip distance minima. Movie versions of this figure are provided in Supporting Information S1 and S2.

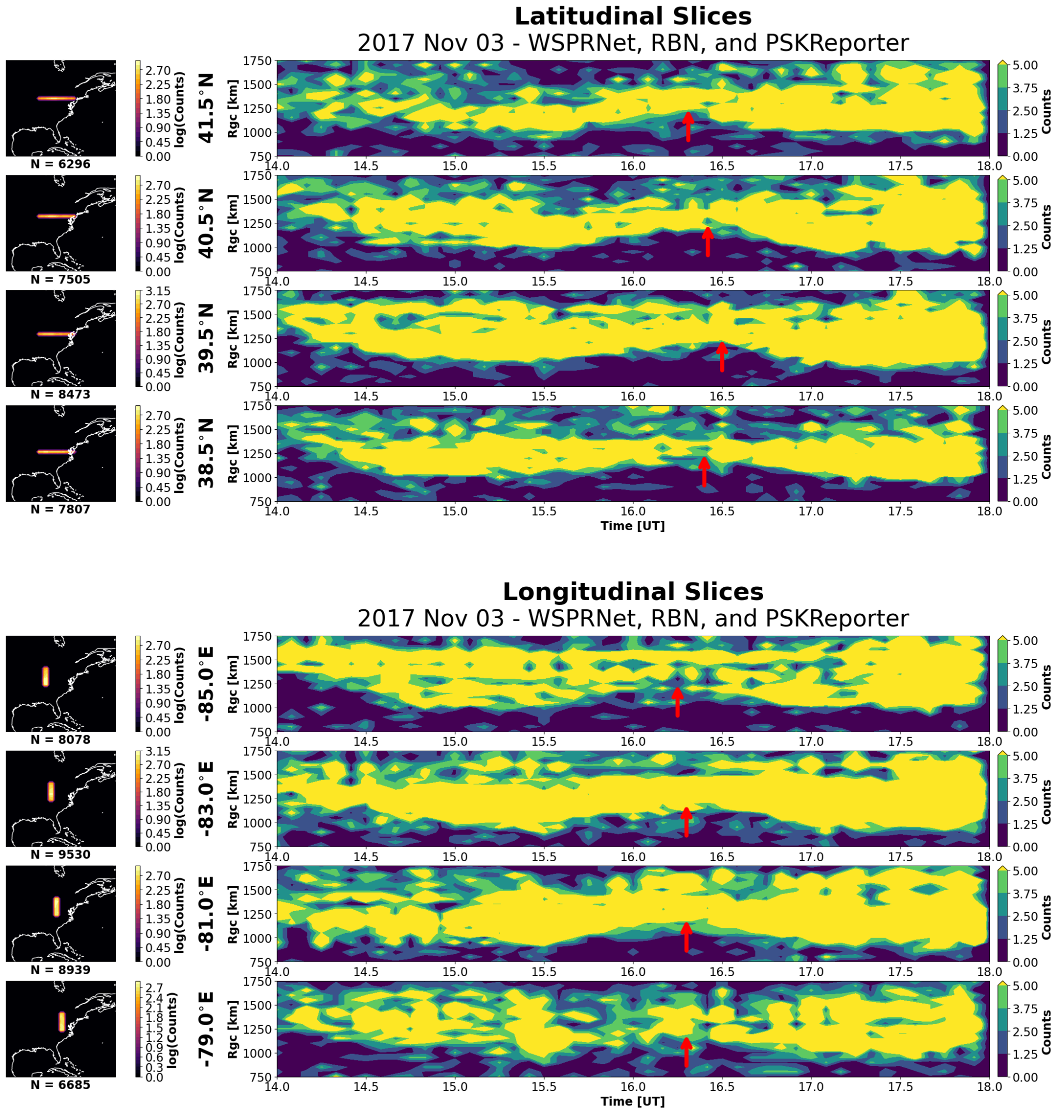

Figure 3. Plots of amateur radio data in latitudinal and longitudinal slices to estimate the phase speed of the LSTIDs. The top four rows show 1° latitudinal slices that range from 42° to 38°N and extend from 88° to 74°W longitude. The bottom four rows show 2° longitudinal slices that range from 85° to 79°W and extend from 37° to 44°N latitude. Red arrows indicate the time of the skip distance maxima manually identified in each time series plot.

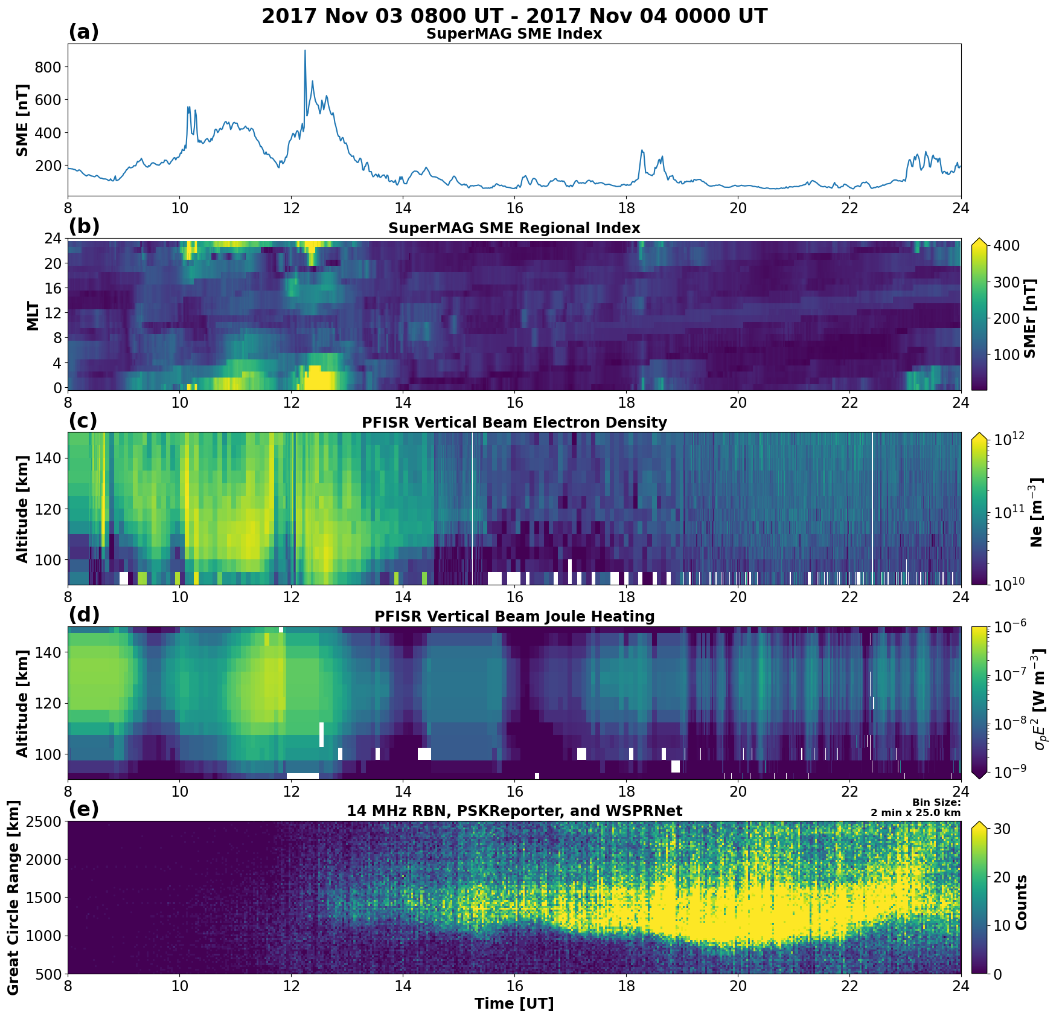

Figure 4. Measurements of auroral zone activity followed by midlatitude amateur radio LSTID observations for 0800 UT 3 Nov 2017 – 0000 UT 4 Nov 2017. (a) SuperMAG Electrojet (SME) Index. (b) Regional SuperMAG Electrojet Index. (c) Poker Flat Incoherent Scatter Radar (PFISR) vertical beam electron density measurements. (d) PFISR vertical beam Joule heating measurements. (e) Time series showing the TX-RX distance for continental U.S. 14 MHz RBN/WSPRNet/PSKReporter amateur radio spots in 2 min by 25 km bins.